Postprint of: Dettlaff A., Sobaszek M., Klimczuk T., Bogdanowicz R., Enhanced electrochemical kinetics of highly-oriented (111)-textured boron-doped diamond electrodes induced by deuterium plasma chemistry, CARBON (2020), DOI: 10.1016/j.carbon.2020.11.096

Enhanced electrochemical kinetics of highly-oriented (111)-textured boron-doped diamond electrodes induced by deuterium plasma chemistry

Anna Dettlaff[a,b,], Michał Sobaszek[b,*], Tomasz Klimczuk[c], and Robert Bogdanowicz[b]*

[a]*Gda sk University of Technology, Faculty of Chemistry, Department of Energy Conversion and Storage, 11/12 Narutowicza Str., 80-233 Gda sk, Poland*
[b]*Gda sk University of Technology, Faculty of Electronics, Telecommunications and Informatics, Department of Metrology and Optoelectronics, 11/12 Narutowicza Str., 80-233 Gda sk, Poland*
[c]*Gda sk University of Technology, Faculty of Applied Physics and Mathematics and Advanced Materials Centre, Department of Solid State Physics, 11/12 Narutowicza Str., 80-233 Gda sk, Poland*

Abstract

Novel highly-oriented (111)-textured boron-doped diamond electrodes (BDD_D) featuring high electrochemical activity and electrode stability toward electrochemical analytics were fabricated by deuterium-rich microwave plasma CVD. The high flux deuterium plasma-induced preferential formation of (111)-faceted diamond as revealed by XRD. The highly-oriented diamond surface exhibited improved boron dopant incorporation and activation, whereas the crystals showed enhanced carrier electron acceptance and donation, which accelerated the electron transfer during electrochemical redox mediation. The standard rate constant and peak-to-peak separation ΔE for the oxidation and reduction of the $Fe(CN)_6^{3-/4-}$ and $Ru(NH_3)_6^{2+/3+}$ redox probes reached ΔE values of only 60.6 and 59.8 mV, respectively. The enriched electrochemical performance of the BDD_D electrodes is an advantageous feature allowing them to be applied as ultrasensitive electrodes, demonstrated here by paracetamol determination. The differential pulse voltammetry results revealed an enhanced electrochemical oxidation effect for paracetamol at the deuterium-grown (111)-rich diamond electrode. A single linear range from 1 to 125 M along with a low detection limit of 0.76 M were achieved.

Keywords: *deuterium plasma, boron-doped diamond, cyclic voltammetry, electrochemical sensors, paracetamol*

[*]*Corresponding Authors. Tel. +48 58 347 1503, +48 58 347 1931.*
E-mail: anna.dettlaff@pg.edu.pl, michal.sobaszek@pg.edu.pl

1. Introduction

Boron-doped diamond (BDD) has aroused the interest of scientists from around the world due to its remarkable properties such as its wide electrochemical potential window, chemical stability and inertness, and biocompatibility, among others [1–4]. Diamond films are grown mainly from a gas phase consisting of hydrogen, carbon, and a dopant source by microwave plasma-assisted chemical vapour deposition or hot filament chemical vapour deposition. The gas composition during the growth has a significant influence on the surface morphology and the electrochemical properties of the BDD films [5,6], especially the dopant concentration, surface defects, and superficial non-diamond carbon phases (NDC) [1].

It is well known that hydrogen radicals play a crucial role in high-quality diamond growth through etching NDC [7,8]. The etching of the diamond sp^3 phase is much slower than the sp^2 or sp phases. Due to deuterium radicals having twice the mass of hydrogen radicals, the process of etching is accelerated resulting in reduced growth rate [9].

The electrochemical properties of boron-doped diamond electrodes depend on factors such as the boron doping concentration, surface termination, and interactions of superficial non-diamond phases. Granger and Swain [1] studied the influence of surface interaction using the $Fe(CN)_6^{-3/-4}$ redox couple. The study results showed that the number of sp^2 phases, and surface termination by hydrogen and oxygen had a crucial impact on BDD's electrochemical properties. Moreover, Garcia-Segura et al. investigated the role of sp^3/sp^2 on the electrocatalytic properties, which has an impact on the potential window, pollutant mineralisation etc. [5].

In the literature, research efforts to enhance the boron doping can be found, which have resulted in improvements of the electronic properties which allows the doped polycrystalline diamond to be used in electronics. Teraji *et al.* [10] grew homoepitaxial diamonds (100) using high-pressure high-temperature type-Ib (100) diamond single crystal substrates to achieve a low resistance of around 1 ohm·cm by the high-power Microwave Plasma Assisted Chemical Vapor Deposition (MW PACVD) process. In the case of single-crystal diamond films, the high-power conditions are responsible for enhanced (of about one order of magnitude) boron-incorporation efficiency, resulting in a carrier concentration of $6 \cdot 10^{15}$ cm^{-3}. Wang *et al*. [11] used Ar-rich or H_2-rich source-gas mixtures to synthesise heavily boron-doped nanocrystalline diamond films with equivalent electrical and electrochemical properties. Furthermore, Issaoui *et al*. [12] showed

that the microwave power density is one of the key factors allowing the doping efficiencies to be tuned over a range of two orders of magnitude.

In our recent study, we investigated the plasma composition by optical emission spectroscopy during diamond film synthesis in a deuterium and hydrogen plasmas [9]. Moreover, we showed enhanced boron doping in the MW PACVD process using deuterium, achieving one order of magnitude higher charge carrier density for BDD_D (deuterium boron-doped diamond) than for BDD_H (hydrogen boron-doped diamond).

Here, we report electrochemical studies of as-grown boron-doped diamond thin-film electrodes, synthesised in a deuterium-rich plasma, by means of cyclic voltammetry and electrochemical impedance spectroscopy. To the best of our knowledge, the effect of replacing hydrogen by deuterium during BDD growth on the electrochemistry of this material has not been reported. Thus, we have performed the electrochemical evaluation of BDD_D including the standard rate constant (k°), and peak-to-peak separation values for the oxidation and reduction of the $Fe(CN)_6^{3-/4-}$ and $Ru(NH_3)_6^{2+/3+}$ redox mediators. Moreover, we also conducted the electrochemical detection of paracetamol via differential pulse voltammetry. The surface morphology, chemical composition, crystallographic orientation and sheet resistivity of the grown BDD_D electrodes were also investigated along with electrochemical techniques.

2. Experimental section

2.1 Diamond growth

The BDD_D and BDD_H were synthesised in the Microwave Plasma Assisted Chemical Vapour Deposition process. Diamond films were deposited on p-type (100) silicon substrates (1 x 1 cm^2). The substrates were cleaned in acetone in an ultrasonic bath for 5 minutes, and then washed in 2-propanol. The substrates were then sonicated in a water nanodiamond suspension (NanoAndo, Japan). A D_2/CH_4 or H_2/CH_4 gas mixture of 1% vol. At an overall gas flow rate of 300 sccm was used for the diamond film synthesis. The temperature of the heated stage was set to 700°C, the process pressure to 50 Torr (6.7 kPa), and the microwave power to 1300 W. Diborane (B_2H_6) was used as a boron source. The boron doping level, expressed as the [B]/[C] ratio in the gas phase, was set to 10k ppm [9]. The growth times of the BDD_D and BDD_H films were adjusted to achieve similar layer thicknesses, so the BDD_D was grown 6 hours, and the BDD_H for 2.5h,

producing microcrystalline films with an average thickness of 650 nm and 690 nm, respectively. The cooling process took place in the CVD reactor in the constant flow of deuterium or hydrogen gas (100 sccm) at a reduced pressure of p=25 Torr. The samples were removed from the reactor when the temperature of 25°C was reached.

2.2 Characterisation techniques

XRD&SEM: *X-ray diffraction (XRD) analysis on the silicon plates with the deposited diamond film was carried out on a Bruker D8 Advance Eco diffractometer with Cu K radiation and a LynxEye-XE detector. The data were collected for 2θ range 42-46 deg. and 74-77 deg. where (111) and (220) reflections are observed. Scanning electron microscope (SEM) micrographs were captured using a Hitachi S-3400N microscope, operating in secondary electron mode at a 25 kV accelerating voltage.*

Raman spectroscopy: *The investigation of the molecular composition of the electrodes was carried out by means of Raman spectroscopy. A Horiba LabRAM ARAMIS Raman confocal microscope (100×/0.95 objective, 50 m of confocal aperture) equipped with a 532 nm diode-pumped solid-state (DPSS) laser was used.*

Electrochemical measurements: *The electrochemical properties of the BDD_D and BDD_H electrodes were investigated by cyclic voltammetry (CV), electrochemical impedance spectroscopy (EIS), and differential pulse voltammetry (DPV) using a potentiostat–galvanostat (VMP-300, Bio-Logic, France) with the EC-Lab software. All electrochemical measurements were conducted in a three-electrode electrochemical cell. The Pt wire served as the counter electrode, while Ag/AgCl and Ag/AgCl/3M KCl electrodes were the reference electrodes. The geometric surface area of the working electrode was 0.196 cm^2. Prior to the electrochemical measurements, the solutions were deoxygenated with argon. The cyclic voltammetry was carried out in contact with aqueous 5 mM potassium ferricyanide (III) and 5mM hexaammineruthenium (III) chlorides, both in 0.5 mol dm^{-3} of Na_2SO_4 solution with an applied scan rate from 5 to 300 mV s^{-1}. The electrochemical impedance spectra were recorded across a wide frequency range from 0.015 Hz to 100 kHz in 5 mM $K_3[Fe(CN)_6]$ with 0.5 M Na_2SO_4, and in 5 mM $[Ru(NH_3)_6]Cl_3$ in 0.5 M Na_2SO_4 solutions at a formal potential (held for 5 min) with a peak-to-peak amplitude of 10 mV and 6 points per frequency decade. The BDD_D electrode was also tested in 0.625 mM, 1.25 mM, 2.5 mM, 3.75 mM and 5 mM $K_3[Fe(CN)_6]$ concentration with 0.5*

M Na_2SO_4 at 50 mV s^{-1}. The DPV measurement parameters were optimised as a pulse height of 60 mV, a pulse width of 70 ms, a step time of 1000 ms, and a scan rate equal to 5 mV s^{-1} (see Fig. S1). The potential ranged from 0.3 to 0.9 V (vs. Ag/AgCl/3.0 M KCl).

Wettability: *Angle was measured by the sessile drop method (drop volume ~50 L) using a self-designed tensiometer system based on a B/W CCD camera (Thorlabs, DCU223 M, USA). Determination of the angle between the BDD surface and the tangent of the drop was performed using MATLAB 6.0 (The MathWorks, USA). The contact angle was measured in three different spots, and for both sides of the drop.*

2.3 Preparation of PCM solutions

For the DPV analyses, the standard stock solution of 1 mM of paracetamol (PCM) concentration was prepared in 0.1 M of phosphate buffer solution (PBS) with pH = 7. Then an aliquot volume of the standard stock solution was added to the appropriate volume of 0.1 M of PBS. The DPV measurements were conducted in 1 mL of sample solution consisting of 0 (background), 0.001, 0.002, 0.004, 0.008, 0.016, 0.032, 0.065, 0.125, 0.25, 0.5, and 1 mM of PCM.

3. Results and discussion

3.1 Physicochemical characterisation of boron-doped diamond surfaces

Experimental Raman spectra are shown in Figure 1a. The sp^3 diamond lines are located at 1331 and 1313 cm^{-1} for the BDD_H and BDD_D, respectively. The boron-doping affects the diamond line causing a shift towards lower wavenumbers. Additionally, for BDD_D, the sp^3 peak is strongly asymmetric which is attributed to the Fano effect [13], a result of interference between the scattering by the zone-centre phonon line and the scattering by an electronic continuum [14,15]. It is worth notice that only for BDD_D, we can see two broad peaks located at ca. 500 and 1200 cm^{-1} which are attributed to the incorporation of boron in the diamond lattice [16]. According to the literature, these two broad bands are attributed to the maxima of the phonon densities of the states [17]. For both samples, peaks assigned to the first order of silicon are visible, located at 520 cm^{-1} for one-phonon mode, and the second-order of silicon is visible at 970 cm^{-1} in both cases.

Additionally, the Fano-shaped peaks located at ca. 500 cm^{-1} (BWF function #1), 1200 cm^{-1} (BWF function #2), and 1312 and 13331 cm^{-1} (BWF function #3) were modelled using the Breit-Wigner-Fano function (see Eq. (1)) [15,18] which is shown in Figure 1 b–c.

$$F_i(\omega) = \frac{A_i \times \left(q_i + \frac{\omega - \omega_i}{\Gamma_i}\right)^2}{1 + \left(\frac{\omega - \omega_i}{\Gamma_i}\right)^2} \qquad (1)$$

In the equation, A_i is the amplitude of the Fano-shaped peaks, q_i is the asymmetric parameter, $_i$ is the width, and $_i$ is the position of the lines.

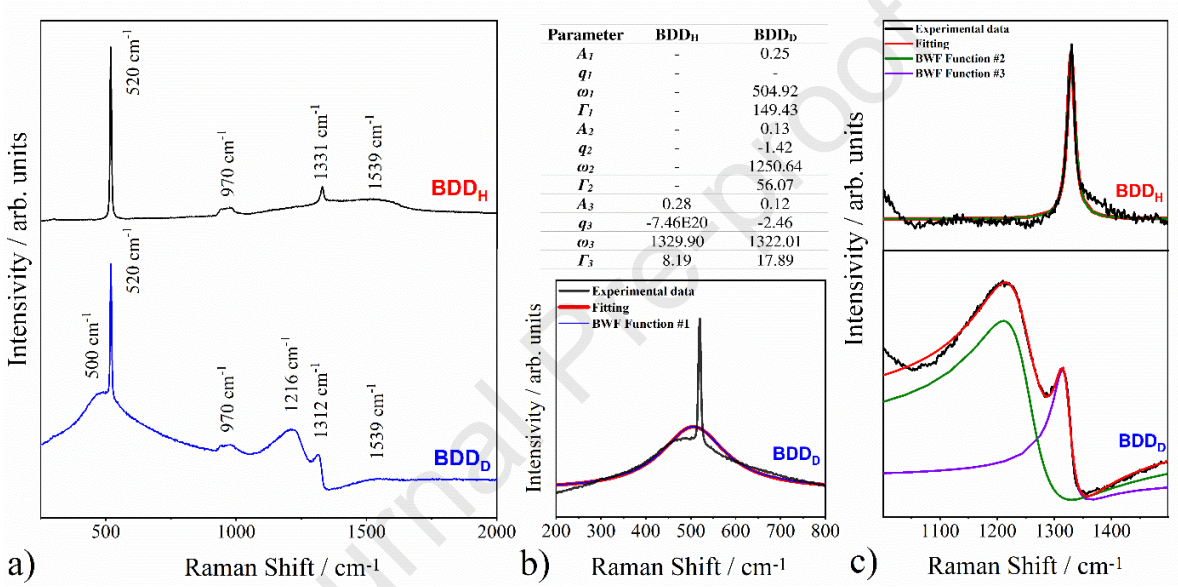

Fig. 1. *a) Normalised raw Raman spectra of BDD$_H$ and BDD$_D$ electrodes, b) and c) normalised Raman spectra modeled using Breit-Wigner-Fano function, fitting (red line), different Fano-shaped peaks (BWF #1 blue line, BWF #2 green line, BWF #3 purple line); Table: Fitting parameters of BDD$_H$, and BDD$_D$ electrodes. Indices 1, 2, and 3 correspond to the BWF#1, BWF#2, and BWF#3 bands, respectively.*

The fitting parameters are shown in Fig. 1b. In the case of the BDD$_H$, the sample's time adjustment (to have similar thickness) result in low boron incorporation into the diamond lattice that in turn results in a lack of BWF#1 and BWF#2 bands. The amplitudes of the Fano-shaped sp^3 (BWF#3) peak is lower for the BDD$_D$, and the peak width ( ) is wider, which is attributed to more boron incorporation into the diamond lattice [15]. According to an investigation by Mortet et al. [18], the asymmetric parameter of the diamond sp^3 line (q_3) can be used as a marker of the

carrier concentration. Only the BDD_D sample indicated significant asymmetry (BDD_D q_3=-2.46), and it should be noted that the q_3 value of the BDD_D electrode proves the high incorporation of boron atoms when deuterium-rich plasma is used.

Noteworthy, BDD_D shows a low amount of sp^2 phase despite the high boron concentration in the diamond lattice. Usually, the high boron content in the diamond film increases the amount of sp^2 phase as a result of degeneration of diamond lattice [19]. In the case of BDD_H sample, the sp^2/sp^3 ratio reaches 0.96% which is typical for a low doped diamond film and the BDD_D sp^2/sp^3 ratio reaches 0.82%. For the estimation of the sp^2/sp^3 ratio was used the McNamara et al. formula taking into account the cross-sections of the Raman signals of sp^3 and sp^2 peaks [20,21]. The formula is given by Eq. (2),

$$sp^2\Big/_{sp^3} = 100 \text{ x } I_G/(75 \cdot I_{diam} + I_G) \qquad (2)$$

where I_{diam} is the intensity of diamond peak while I_G means the intensity of the G band. Swain and Ramesham [22] reported the sp^2 phase content extending from 1 to 5% in BDD electrodes. Xu et al. [23] showed that the I_G/I_{Diam} quantitative ratio equals 0.04 for the diamond samples with 1% of boron. The grain size in this sample was ca. 8.3 µm, while reported here BDD_D electrodes exhibit grains of avg. 0.5 µm. It should be noticed that the sp^2 is predominantly localized in the inter-grain regions [24].

It was previously demonstrated that the propensity to oxidation is inseparably correlated with BDD's crystallographic texture *[25–27]*. SEM images presented in Fig. 2a) and 2b) reveal on average two times larger grains of BDD_D than BDD_H, which results in a reduced doping impact on the grain size in the case of deuterium-rich plasma synthesis. The BDD_D grains are smooth and sharp, while the BDD_H grains are degraded due to the dominance of the number of non-diamond sp^2 phases *[28,29]*. According to the SEM analysis, the thickness of the BDD_D and BDD_H can be approximated to ~645 and ~690 nm, respectively. Authors kept a similar thickness of both samples to compare them. To achieve that, the different growth times of BDD_D and BDD_H were applied. It was previously found that synthesis in deuterium-rich plasma results in the growth rate of about twice as slow in comparison with hydrogen-rich conditions [9]. The deuterium has higher mass resulting from the more intensive etching of the diamond and non-diamond forms [9,30]. The Raman result also confirms Hall effect measurements resulting in one

order of magnitude higher holes concentration in BDD_D reaching over 10^{20} cm^{-3} and 10^{19} cm^{-3} for BDD_H [9], respectively.

The SEM micrographs reveal a significantly altered crystallographic orientation of the surface BDD grains, which was further examined through XRD studies. The crest-like grain boundaries of (111) and (220) microfacets constitute the BDD_H electrode surface. On the other hand, the BDD_D electrode's surface is dominated by nearly flat and crystallite edges of (111) microfacets.

The XRD analysis confirms the SEM crystallographic orientation results (see Fig. 2c-d). Only two XRD reflections of the nanodiamond films were found on the XRD patterns. Comparing the (111) reflections observed at 2θ = 49.3, we conclude that the BDD_D sample has a twice more intense reflection than the BDD_H sample. This phenomenon has a crucial impact on the electrical and electrochemical properties as the (111) plane is the most promoted to the incorporation of boron atoms [31–33]. Furthermore, the intensity of the (220) plane located at 75.2 and 75.5 is far stronger for the BDD_H than for the BDD_D, which is less promotive to the boron doping and more degenerate. For a randomly oriented polycrystalline diamond powder, the theoretical value of the $I_{(220)}/I_{(111)}$ ratio is 0.25 according to ASTM powder diffraction data. The $I_{(220)}/I_{(111)}$ ratio for the BDD_H is 2.16, and 0.06 for the BDD_D, indicating that the texture of the BDD_H electrode film is oriented along the (220) direction and the BDD_H along the (111) direction.

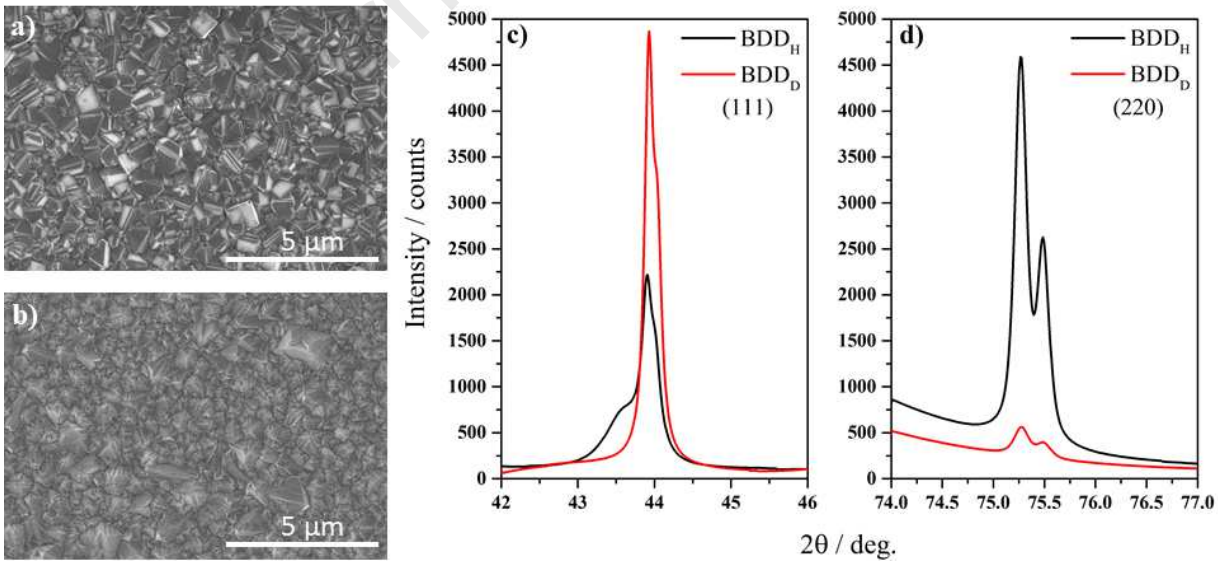

Fig. 2. *SEM micrographs of a) BDD_D, and b) BDD_H with 10000x, and XRD patterns of c) (111), and d) (220) crystallographic planes.*

Next, the electrical properties of the BDD_H and BDD_D electrodes were measured with a four-point probe system. The average resistivity for the sample deposited in hydrogen-based plasma was 0.08 ·cm, and 2.6 m ·cm for deuterium, which resulted in conductivities equal to 12.5 and 384.6 $S \cdot cm^{-1}$, respectively. The lower resistance of the BDD_D sample could be attributed to the direct charge transfer along the large grains, and tunneling in the intergrain region [34]. Furthermore, the lower electrical resistivity achieved for BDD_D was a result of the slightly bigger grains, which corresponds to a study reported by Habka et al.[34] in which the authors show that the grain size of polycrystalline diamond is the key parameter for efficient deuterium diffusion and trapping of boron atoms. In comparison to the BDD_H samples, we achieved one order of magnitude lower resistance for the BDD_D which is in agreement with our previous investigation showing enhanced boron-doping where the sample is grown in deuterium-rich plasma [9]. On the other hand, we achieved the same level of electrical resistivity for boron-enhanced carbon nanowalls [35] which is a hybrid material consisting of graphene nanowalls overgrown by nanodiamond clusters.

It is obvious that the variations in the isotopic composition of growth precursors drastically changes properties of deposited solid phase inducing mostly proton enhanced kinetics [36]. To improve the stoichiometric composition, the bulk diamond crystals were additionally annealed in deuterium at 500 - 550°C [37]. *Mizuochi et al. [38] revealed that the energy of molecules and atoms in the D_2 plasma are higher than those in the H_2 plasma, while the etching rate by D is about 20% larger than that by H in this condition.*

The contact angle was measured for the as-deposited samples (see Fig. S2). Both samples showed similar hydrophobicity with slightly higher values for the BDD_H samples. The recorded contact angle for the BDD_H was 94.5° and for the BDD_D was 85.7°. The measured angles are in agreement with other works [39,40]. The almost 10° difference between the contact angle can be explained by the difference in crystallite size and facet, which be determined by the amount of the surface termination by hydrogen or deuterium, resulting in different free surface energies [41].

3.2 Electrochemical studies: BDD_D versus BDD_H

Cyclic voltammetry testing of the bare BDD_D and BDD_H electrodes in a neutral electrolyte (0.5 M Na_2SO_4) was performed to examine the electrochemical potential window (EPW), and

the magnitude of the background current. The results are presented in Fig. 3. As can be seen, a low background current value and very wide working potential windows (up to 3.8 V) can be observed for both diamond electrodes. However, the BDD_H layer is unstable at a deep cathodic potential (below -1.6 V), whereas the BDD_D can be polarised to -1.8 V. Wider EPW of deuterium boron-doped diamond may be caused by lower amount of sp^2 when compared to the BDD_H electrode [42]. Furthermore, the presence of non-diamond carbon in both electrodes is confirmed by a weak cathodic peak at ca. -0.85 V, which may be assigned to the oxygen reduction reaction [33]. The wide EPW is related to the overvoltage of water decomposition. The oxygen electrode reaction and the hydrogen electrode reaction belong to the inner-sphere reaction. The rates of such reactions depend on the electrode surface structure (the reactions require the adsorption process of the reaction intermediates) [43]. Thus, a wide EPW value of water stability indicates a high-quality diamond layer with a low number of defects and grain boundary density [2,44].

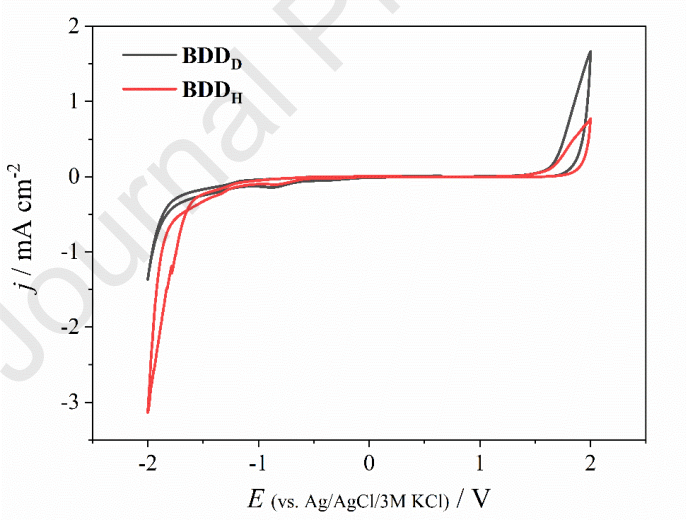

Fig. 3. *Cyclic voltammetry of BDD_D and BDD_H electrodes immersed in 0.5 M Na_2SO_4; scan rate 100 mV s^{-1}.*

The electrochemical reactivity of the BDD_D and BDD_H electrodes was investigated using electroactive species characterised with differently charged inner-sphere and outer-sphere electron transfer: 5 mM $K_3[Fe(CN)_6]$ in 0.5 M Na_2SO_4, and 5 mM $[Ru(NH_3)_6]Cl_3$ in 0.5 M Na_2SO_4, respectively. Both potassium ferricyanide (III) and *hexaammineruthenium (III) chloride*

undergo a one-electron reversible redox reaction. The $Ru(NH_3)_6^{2+/3+}$ redox couple represents the outer-sphere redox reaction and the kinetics of the electron transfer does not depend on the interaction with superficial functional moieties. Thus, the adsorbed sp^2 carbon layers, the surface microstructure, and the surface oxides have relatively little influence on the rate of the reaction of $Ru(NH_3)_6^{2+/3+}$ oxidation and reduction. However, the rate of the reaction depends on the electronic features of the electrode, especially the density of the electronic states [2,45]. The $Fe(CN)_6^{3-/4-}$ redox mediator, in turn, belongs to the inner-sphere redox reaction. The $Fe(CN)_6^{3-/4-}$ redox reaction is accompanied by the break-up and formation of the inner coordination sphere. Such reactions usually involve the adsorption process on the electrode surface and strongly depend on the surface chemistry of diamond, because the transfer of the electron requires direct interactions with the reactive sites on the electrodes [2,33,46]. The cyclic voltammetry of both redox systems recorded on BDD_D is presented in Figure 4, whereas the results of BDD_H are shown in Fig. S3.

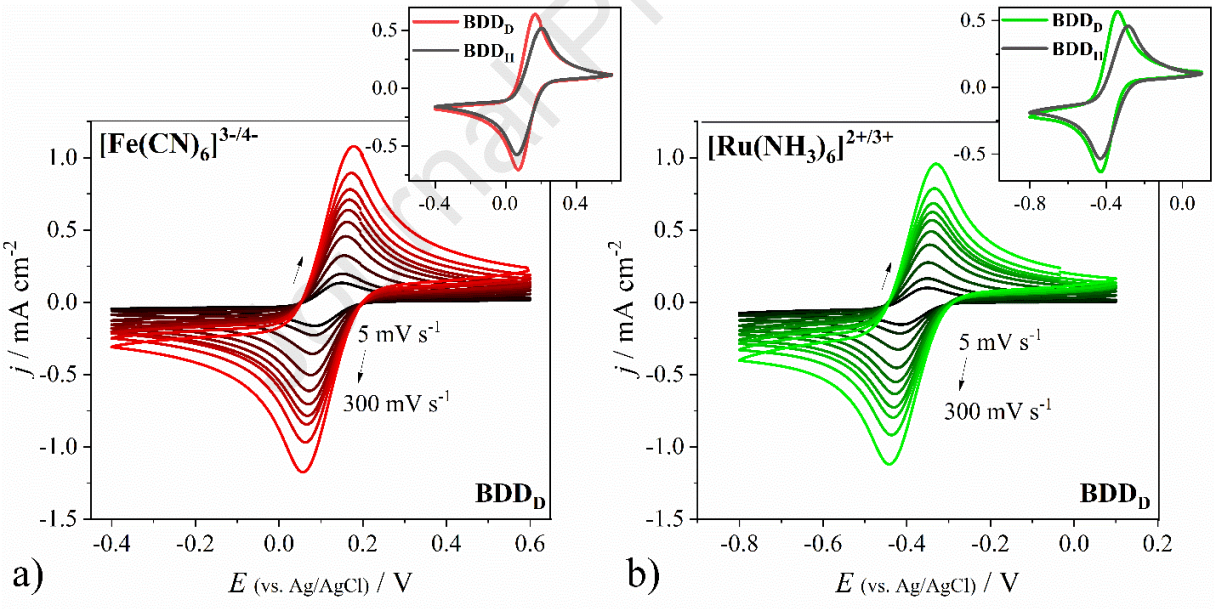

Fig. 4. *CV curves of BDD_D electrodes immersed in: a) 5 mM $K_3[Fe(CN)_6]$ + 0.5 M Na_2SO_4 (inset: BDD_D vs. BDD_H electrode at 100 mV s^{-1}); and b) 5 mM $[Ru(NH_3)_6]Cl_3$ + 0.5 M Na_2SO_4 as a function of scan rates (inset: BDD_D vs. BDD_H electrode at 100 mV s^{-1}).*

In our case, the deuterium-terminated boron-doped diamond electrode exhibited extraordinary peak-to-peak separation values (E) in both $Ru(NH_3)_6^{2+/3+}$ and $Fe(CN)_6^{3-/4-}$ redox couple (Table

1). The E value obtained for 10 mV s^{-1} $Ru(NH_3)_6^{2+/3+}$ was equal to 60 mV, which is expected for a Nernstian one-electron reaction. The separation between the oxidation and reduction peak potentials obtained on the BDD_D electrode increased with the rising scan rate from 60 mV to 114 mV for $Ru(NH_3)_6^{2+/3+}$, and from 61 mV to 121 mV for the $Fe(CN)_6^{3-/4-}$ redox system. The narrow peak-to-peak separation indicates that the BDD_D electrode showed desirable electronic properties and surface structure, which supported fast electron transfer for both: inner- and outer-sphere redox systems. However, better catalytic properties were observed for the $Ru(NH_3)_6^{2+/3+}$ redox probe. Worse catalytic effect of BDD electrodes towards surface-sensitive $Fe(CN)_6^{3-/4-}$ redox mediator can be explained by the presence of edge plane on sp^2 carbon and surface defects on BDD electrodes [44,46]. Increasing peak-to-peak separation at high scan rates may be due to the presence of the Ohmic potential drop [47,48] the presence of which is confirmed by the voltammogram in Fig. S4.

It is known that the anodic and cathodic peaks should be independent of the scan rate for a reversible redox reaction [49]. For the BDD_D electrode response, there was a slight shift in the peak maximum with the increasing sweep rate. The results suggest that the interfacial charge transfer was rather fast for both redox couples and the redox couples behaved in a quasi-reversible manner (the redox reactions were limited by the slow mass transfer of the reactants from the solution to the surface of the electrode).

Table 1. Values of oxidation (E_{ox}) and reduction potentials (E_{red}) and the resulting peak-to-peak separation depending on the scan rate.

	$Fe(CN)_6^{3-/4-}$		**$Ru(NH_3)_6^{2+/3+}$**	
	BDD_D	BDD_H	**BDD_D**	BDD_H
ν / mV s^{-1}	***ΔE* / mV**	*ΔE* / mV	***ΔE* / mV**	*ΔE* / mV
5	**61 ± 1**	73 ± 4	**60 ± 1**	77 ± 3
10	**66 ± 2**	77 ± 5	**65 ± 2**	87 ± 5
25	**74 ± 1**	100 ± 5	**70 ± 1**	107 ± 4
50	**82 ± 0**	115 ± 3	**80 ± 0**	126 ± 6
75	**89 ± 3**	130 ± 5	**86 ± 1**	139 ± 6
100	**95 ± 1**	141 ± 2	**89 ± 2**	151 ± 7
125	**98 ± 2**	147 ± 1	**93 ± 3**	160 ± 8
150	**103 ± 1**	154 ± 1	**97 ± 1**	166 ± 7

200	**110 ± 3**	167 ± 1	**102 ± 3**	182 ± 7
300	**121 ± 2**	184 ± 2	**114 ± 3**	203 ± 6

The BDD_D electrode's almost linear dependence (R^2=0.9995-0.9997), with the zero intercept, of the growth of the anodic and cathodic peak current density with the increasing square root on the scan rate is shown in Fig. 5. A linear dependence of the logarithm of the anodic and cathodic peak current densities vs. the logarithm of the scan rate is also observed (Fig. S5). As can be seen, the cathodic and anodic peak currents increased with the sweep rate. Moreover, there is a symmetry between the oxidation and reduction peaks, which demonstrated a nearly reversible electron transfer reaction. There is a high degree of symmetry of the BDD_D reaction in both electrolyte systems. For $Ru(NH_3)_6^{2+/3+}$ redox mediator, the anodic slope was equal to $4.09 \cdot 10^{-4}$ A $V^{-1/2}$ $s^{1/2}$, while the cathodic was $-4.14 \cdot 10^{-4}$ A $V^{-1/2}$ $s^{1/2}$, whereas for the $Fe(CN)_6^{3-/4-}$ redox couple, the anodic slope was $4.54 \cdot 10^{-4}$ *A $V^{-1/2}$ $s^{1/2}$, and the cathodic was equal to $-4.52 \cdot 10^{-4}$ A $V^{-1/2}$ $s^{1/2}$. Generally, the BDD_H electrode exhibited worse electrochemical behaviour. The value of the peak-to-peak separation increased from 73 to 184 mV for the* $Fe(CN)_6^{3-/4-}$ *redox couple, and from 77 to 203 mV for the $Ru(NH_3)_6^{2+/3+}$ redox system. The slopes* in the $Fe(CN)_6^{3-/4-}$ electron *mediator were equal to $3.72 \cdot 10^{-4}$ A $V^{-1/2}$ $s^{1/2}$ and $-3.73 \cdot 10^{-4}$ A $V^{-1/2}$ $s^{1/2}$, whereas in the $Ru(NH_3)_6^{2+/3+}$ redox couple, the slopes were $3.25 \cdot 10^{-4}$ A $V^{-1/2}$ $s^{1/2}$ and $-3.40 \cdot 10^{-4}$ A $V^{-1/2}$ $s^{1/2}$.* The difference in the electrochemical response of the BDD_D and BDD_H electrodes may be related to the different electrochemical kinetics, which *strongly depends on their boron-doped level, surface termination, diamond grain size, crystallographic orientation, surface resisivity, and presence of NDC impurity phase [1,3,33,43,50]. BDD_D electrode shows much lower surface resistivity, higher boron concentration and lower NDC amount than BDD_H as confirmed by Raman, XRD and CV data. Moreover, works by Zieli ski et al. [51] and Ryl et al. [52] showed the influence of surface termination on the electrochemical performance. Moreover, the crystal configuration also plays a crucial role due to the oxidation propensity sequence (110)>(100)>(111). Also, Invandini et al. [46] investigated the influence of surface orientation on the electrochemical properties and concluded that the (111) plane is more reactive than the (100) plane independent of the type of surface termination (H- and O-). According to work by Brillas and Martinez-Huitle [43], the fastest rates of redox reactions should be observed for the (111) crystal configuration, which refers to the metallic behaviour of the diamond layer. In agreement with the XRD studies, the crystallographic structure of the deuterium-terminated*

diamond is dominated by the (111) configuration. The reactivity of the (111) boron-doped diamond is associated with the high amount of boron built into the carbon structure.

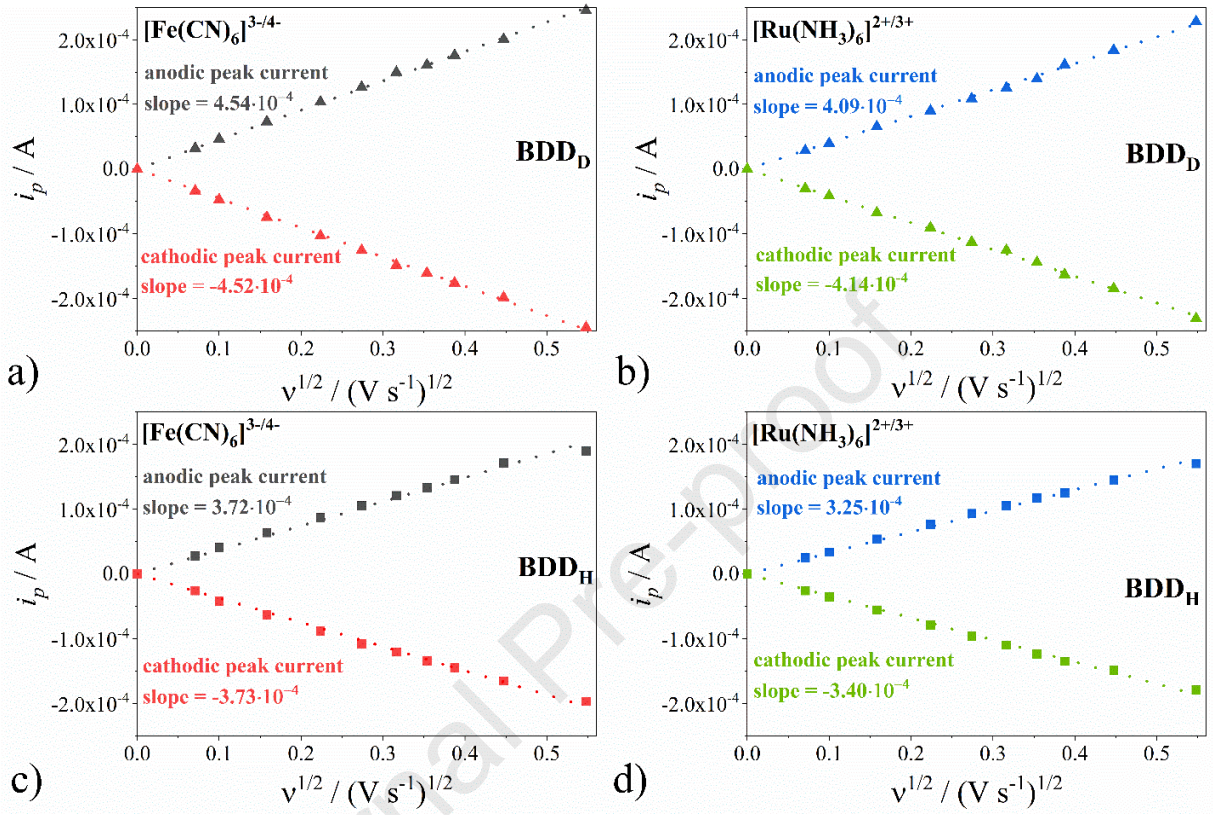

Fig. 5. *Dependence of the peak current on the scan rate obtained for BDD_D electrodes immersed in: a) 5 mM $K_3[Fe(CN)_6]$ + 0.5 M Na_2SO_4; and b) 5 mM $[Ru(NH_3)_6]Cl_3$ + 0.5 M Na_2SO_4; and BDD_H electrodes immersed in: c) 5 mM $K_3[Fe(CN)_6]$ + 0.5 M Na_2SO_4; and d) 5 mM $[Ru(NH_3)_6]Cl_3$ + 0.5 M Na_2SO_4.*

The electroactive surface area of the BDD_D electrode, A_e (cm^2), was calculated using the modified Randles-Sevcik equation for quasi-reversible reactions (2) [53,54]:

$$i_p = 0.4463 \cdot n \cdot F \cdot A_e \cdot C \cdot D^{\frac{1}{2}} \cdot \sqrt{\frac{n \cdot F}{R \cdot T}} \cdot \nu^{\frac{1}{2}} \cdot \kappa(\Lambda, \alpha), \qquad (2)$$

where i_p is the peak current (A), F corresponds to Faraday's constant (96485 C mol^{-1}), R is gas constant (8.314 J K^{-1} mol^{-1}), T is the temperature (298 K), C is the concentration (mol cm^{-3}), D is the diffusion coefficient (cm^2 s^{-1}), n is the number of electrons, is the scan rate (V s^{-1}), κ and are parameters introduced by Matsuda and Ayabe [55], and is charge transfer coefficient

assumed as 0.5 [56,57]. The diffusion coefficients were taken as $7.6 \cdot 10^{-6}$ cm^2 s^{-1}, and $4.96 \cdot 10^{-6}$ cm^2 s^{-1} for $Fe(CN)_6^{4-/3-}$*, and* $Ru(NH_3)_6^{3+/2+}$*, respectively [58,59]. In the* $Ru(NH_3)_6^{3+/2+}$ *redox couple, the determined electroactive surface areas for* BDD_D *and* BDD_H *are equal to 0.14* cm^2 *and 0.11* cm^2*, respectively. In the* $Fe(CN)_6^{4-/3-}$ electron mediator, the A_e values were lower and amounted to 0.12 cm^2 for BDD_D, and 0.10 cm^2 for BDD_H. *There were no differences between the* A_e *obtained for the anodic and cathodic currents in both solutions, which indicates comparable electroactive surface areas regardless of the oxidation and reduction process. The values of* A_e *indicate that 39%, and 29% of the geometric surface area of the* BDD_D *electrode, in* $Fe(CN)_6^{3-/4-}$*, and* $Ru(NH_3)_6^{2+/3+}$*, respectively, were blocked towards electron transfer between the electrode and electrolyte. According to the literature, different polycrystalline crystal faces are incorporated during the growth of boron-doped diamond by chemical vapour deposition. The presence of point defects, non-diamond carbon phases, and grain boundaries may result in heterogeneity in the local concentration of charge carriers [1]. In agreement with the literature, this phenomenon can be explained by heavily overlapping diffusion layers with the characteristics of linear diffusion [60–62]. In this case, the average size of the unblocked areas and the average distance between them are relatively small.*

Electrochemical impedance spectroscopy was carried out in 5 mM $K_3[Fe(CN)_6]$ *with 0.5 M* Na_2SO_4*, and 5 mM* $[Ru(NH_3)_6]Cl_3$ *in 0.5 M* Na_2SO_4 *at the formal potential of the redox reaction for* BDD_D*. Simultaneously, the measurement was also conducted on the reference* BDD_H *electrode. The Nyquist plots are depicted in Fig. 6. Quantitative data were estimated using an electric equivalent circuit (EEQC) in the ZSimpWin analyser software. The EEQC used for fitting* $R_e(CPE(R_{ct}W))$ *is shown in inset Fig. S6. The fitting procedure gave normalised fitting errors* χ^2 *at the level of* 10^{-4}-10^{-3}*. The values of the electrical parameters evaluated using the aforementioned EEQC are collected in Table 2.*

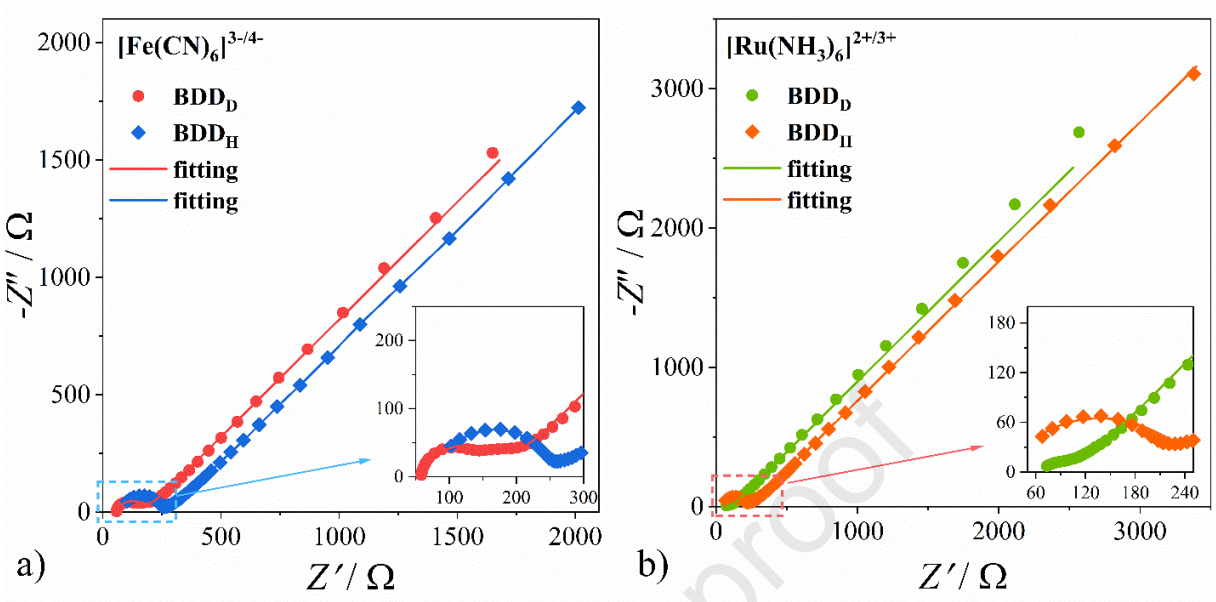

Fig. 6. *Nyquist plots registered and fitted for BDD_D and BDD_H electrodes immersed in: a) 5 mM $K_3[Fe(CN)_6]$ + 0.5 M Na_2SO_4; and b) 5 mM $[Ru(NH_3)_6]Cl_3$ + 0.5 M Na_2SO_4.*

The EIS spectra include a semicircle region lying in the high-frequency regime followed by a straight line with a 45° slope (at a lower frequency). The semicircle represents the electron-transfer-limited process, while the line corresponds to the diffusion-limited process. The electrolyte resistance, R_e, is an element arising in the high-frequency range. The value of R_e is ca. 12 cm^2, and 13 cm^2 for $Ru(NH_3)_6^{2+/3+}$, and $Fe(CN)_6^{3-/4-}$, respectively. *A low electrolyte resistance indicates a good attachment of the BDD_D to the silicon substrate. Furthermore, it suggests a low contamination level of the surface. The charge-transfer resistance R_{ct} is equal to the diameter of the aforementioned semicircle. The R_{ct} value is significantly lower for the BDD_D electrode and is equal to 9.8 $\Omega \cdot cm^2$ in* $Ru(NH_3)_6^{2+/3+}$, *and 18.2 $\Omega \cdot cm^2$ in* $Fe(CN)_6^{3-/4-}$, which *indicates better electron transfer processes. The impedance spectra show that the capacitance of both diamond electrodes depends on frequency. Thus, the electrical equivalent circuit of the electrodes includes a frequency-dependent constant phase element (CPE) which also reflects the distribution of reactivity caused by the surface electrochemical heterogeneity [63–67]. The CPE impedance (Z_{CPE}) is defined as $Z_{CPE} = 1/Q(j\ )^n$, where Q and n are the constant phase element parameters, is the angular frequency, and j is the imaginary number. The Warburg impedance (Z_w) describes a diffusional resistance. This element was used only in terms of the correct fitting procedure of the other elements.*

Table 2. *Mean values of selected electric parameters calculated on the basis of $R_e(CPER_{ct}W)$ equivalent circuit.*

	$Fe(CN)_6^{3-/4-}$		$Ru(NH_3)_6^{2+/3+}$	
	BDD_D	BDD_H	BDD_D	BDD_H
R_{ct} / Ω cm^2	18.2	79.3	9.8	43.9
CPE / Ω^{-1} cm^{-2} s^n	$2.0\cdot10^{-4}$	$1.1\cdot10^{-6}$	$3.9\cdot10^{-4}$	$7.1\cdot10^{-6}$
n	0.8	0.8	0.8	0.8
W / Ω^{-1}*s*$^{0.5}$ cm^{-2}	$5.5\cdot10^{-3}$	$2.4\cdot10^{-3}$	$5.9\cdot10^{-3}$	$4.4\cdot10^{-3}$

The apparent heterogeneous electron transfer rate constant $k°_{app}$ was calculated using Eq. (3) [68,69]:

$$k°_{app} = \frac{R\cdot T}{n^2\cdot F^2\cdot A\cdot C\cdot R_{ct}}, \qquad (3)$$

where R is the molar gas constant (8.32 J mol^{-1} K^{-1}), T is the electrolyte temperature (K), *n* is the number of electrons exchanged during the reaction, *F* is the Faraday constant (96,500 C), *A* is the geometric electrode area, and *C* is the concentration (mol cm^{-3}). The standard rate constant values for the BDD_D were equal to $5.84\cdot10^{-3}$ ($\pm 0.56\cdot10^{-3}$) cm s^{-1} for $Ru(NH_3)_6^{2+/3+}$, and $2.93\cdot10^{-3}$ ($\pm 0.86\cdot10^{-3}$) cm s^{-1} for the $Fe(CN)_6^{3-/4-}$ redox system, respectively. The BDD_H electrode gave a $k°_{app}$ of $1.213\cdot10^{-3}$ ($\pm 0.026\cdot10^{-3}$) cm *s^{-1} for* $Ru(NH_3)_6^{2+/3+}$, and $6.72\cdot10^{-4}$ ($\pm 3.41\cdot10^{-4}$) *cm s^{-1}* for the ferri-ferrocyanide system. *According to work by Alehashem et al. [70], the achieved in* the $Fe(CN)_6^{3-/4-}$ redox system *$k°_{app}$ value is one order of magnitude higher for the BDD_D than for the standard BDD_H resulting in a higher heterogeneous electron transfer rate constants. The value of $k°_{app}$ is heavily dependent on the chemical and physical properties of the diamond-based electrodes [1]. Also, $k°_{app}$ is strongly sensitive to the amount of exposed edge plane on sp^2 carbon electrodes [71]. The high value of $k°_{app}$ indicates a low amount of surface sp^2 phase on the BDD_D, which is in agreement with the Raman spectroscopy investigations.*

The calculated values are in agreement with the standard rate constants found in the literature for boron-doped diamond (from 10^{-5} to 10^{-2} cm s^{-1}) [49,63,71]. Moreover, the value of $k°_{app}$ confirms the reversibility of the electrochemical processes, which should be between 10^{-1} and 10^{-5} cm s^{-1} [49].

Table 3. Comparison of the physicochemical and electrochemical properties of polycrystalline boron-doped diamonds.

Sample	Process	Post-treatment	[B]: [C] ratio / ppm	[B] / B atoms cm^{-3}	Grain size /µm	*R* / mΩ·cm	EPW / V	Δ*E* $Fe(CN)_6^{3-/4-}$ / mV	Δ*E* $Ru(NH_3)_6^{2+/3+}$ /mV	$k°_{app}$ $Fe(CN)_6^{3-/4-}$ / $cm·s^{-1}$	$k°_{app}$ $Ru(NH_3)_6^{2+/3+}$ / $cm·s^{-1}$	Ref.
BDD	MW PACVD	annealed under a N_2 atmosphere	1,100	n/d	1-10	10^4	1.2	104	n/d	n/d	n/d	[72]
BDD	MACVD[1]	aqua reqia; $H_2SO_4/HNO_3/NaNO_3$; H_2 plasma	n/d	10^{19}–10^{20}	3	10^2	1.4	70	70	n/d	n/d	[1]
BDD	MW PACVD	H_2O_2/H_2SO_4; H_2 plasma	10,000	$3.4·10^{17}$–$1.8·10^{21}$	1-2	7	n/d	243	n/d	n/d	n/d	[73]
BDD	MW PACVD	no	600	$1.0·10^{20}$	11	n/d	4.9	980	380	n/d	n/d	[23]
BDD	MW PACVD	H_2SO_4/HNO_3; HNO_3/HCl; HF; H_2 plasma	n/d	$7.6·10^{20}$	5	6	n/d	60	60	n/d	n/d	[46]
BDD	MACVD	$H_2SO_4/HNO_3/NaNO_3$; H_2 plasma	n/d	10^{19}–10^{20}	2-4	10^2	3.8	64	65	10^{-3}–10^{-2}	10^{-3}–10^{-2}	[71]
BDD	HFCVD[3]	H_2 plasma	10,000	n/d	n/d	n/d	2.8	473	61	$1.1·10^{-4}$	$9.7·10^{-2}$	[74]
BDD	Commercial Element Six Ltd	H_2SO_4; lapped	n/d	$1.9·10^{20}$	n/d	60	3.5	n/d	68	n/d	$4.0·10^{-2}$	[75]
BDD	MW PACVD	aqua regia; HNO_3/HCl; H_2O_2/H_2SO_4; H_2 plasma	10,000	$2.0·10^{21}$	n/d	n/d	n/d	108	n/d	$6.1·10^{-3}$	n/d	[63]
BDD	HFCVD	Cathodic treatment HNO_3	5,000	$4.0·10^{18}$	8–4.5	n/d	3.5	68	92	$1.0·10^{-2}$	$1.31·10^{-3}$	[76]
BDD	MW PACVD	n/d	n/d	n/d	0.5-1.5	10-20	n/d	149	n/d	$1.4·10^{-3}$	n/d	[77]
BDD_H	MW PACVD	no	10,000	$1.5·10^{19}$	0.1	0.08	3.5	73	74	$6.7·10^{-4}$	$1.2·10^{-3}$	this work
BDD_D	**MW PACVD**	**no**	**10,000**	**$7.9·10^{20}$**	**0.5**	**2.6**	**3.8**	**61**	**59.4**	**$2.9·10^{-3}$**	**$5.8·10^{-3}$**	**this work**

[1] Microwave assisted chemical vapour deposition; [2] Plasma assisted chemical vapour deposition; [3] Hot filament chemical vapour deposition

Table 3 enumerates a detailed list of parameters of different polycrystalline boron-doped diamond electrodes reported in the literature comparing them with as-grown BDD_D surfaces. The cleaning, pre-treatment, boron content and structure morphology clearly affects electrochemical parameters like EPW value, peak-to-peak separation, etc.. The most of reported diamond electrodes were subjected to a multi-step cleaning process using an aggressive chemical like hot aqua regia or concentrated, hot sulfuric acid (VI). Xu et al. used "as grown" BDD electrode, but as a result the oxidation and reduction reactions were sluggish ($\Delta E_{[Fe(CN)6]3-/4-}$ = 980 mV, $\Delta E_{[Ru(NH3)6]2+/3+}$ = 380 mV) [23].

3.2.1 Electrochemical determination of paracetamol

The as-deposited BDD_D and BDD_H electrodes were used as an electrochemical sensor for the detection of paracetamol. The DPV technique was used for this purpose. The oxidation peak of the analyte was presented at about +0.49 V (vs. Ag/AgCl/3M KCl). The anodic peak currents of PCM recorded on both types electrode were linear to theirs concentrations in a wide linear range from 1 to 125 μM in 0.1 M PBS (pH 7) (see Fig. 7). The additional anodic peak at ca. +0.62 V of PCM oxidation was observed for both electrodes for high-concentrated samples (see Fig. S7), which can be attributed to by-products of PCM electropolymerisation [4].

Both electrodes exhibited a wide linear range from 1 to 125 μM, and the corresponding linear regression equations were given as i_p [μA] = (72.19 ± 0.92) c_{PCM} [mM] for BDD_D (correlation coefficient = 0.9993) and i_p [μA] = (55.55 ± 0.98) c_{PCM} [mM] for BDD_H (R^2 = 0.9987). Thus, the electrodes differ in the sensitivity of PCM detection, which was equal to 367.85 ± 4.69 μA mM^{-1} cm^{-2} for BDD_D electrode and 283.06 ± 4.99 μA mM^{-1} cm^{-2} for BDD_H electrode. The limit of detection (LOD) was estimated using the equation LOD=3.3 $_{bl}$/a, where is the standard deviation of a blank solution (based on 10 blank readings), and a denotes the slope of the calibration curve [78–80]. The value of LOD calculated for the BDD_D electrode was 765 nM, whereas for the BDD_H was 2510 nM. Moreover, the relative standard deviation (RSD), obtained for five separated BDD_D electrodes used for 125 μM PCM determination, was equal to 5.5%. These results indicate that BDD_D electrode exhibits significant electrocatalytic activity towards paracetamol. Furthermore, BDD_D electrode shows better sensing performance towards PCM comparing to BDD_H electrode. The difference in the behaviour of the electrodes may result from

the higher amount of electroactive zones on deuterium-terminated diamond strictly related to (111) crystal facets [46,81].

Table 4 presents a comparison of the PCM detection performances from the present and previously reported electrochemical sensors on different diamond electrodes.

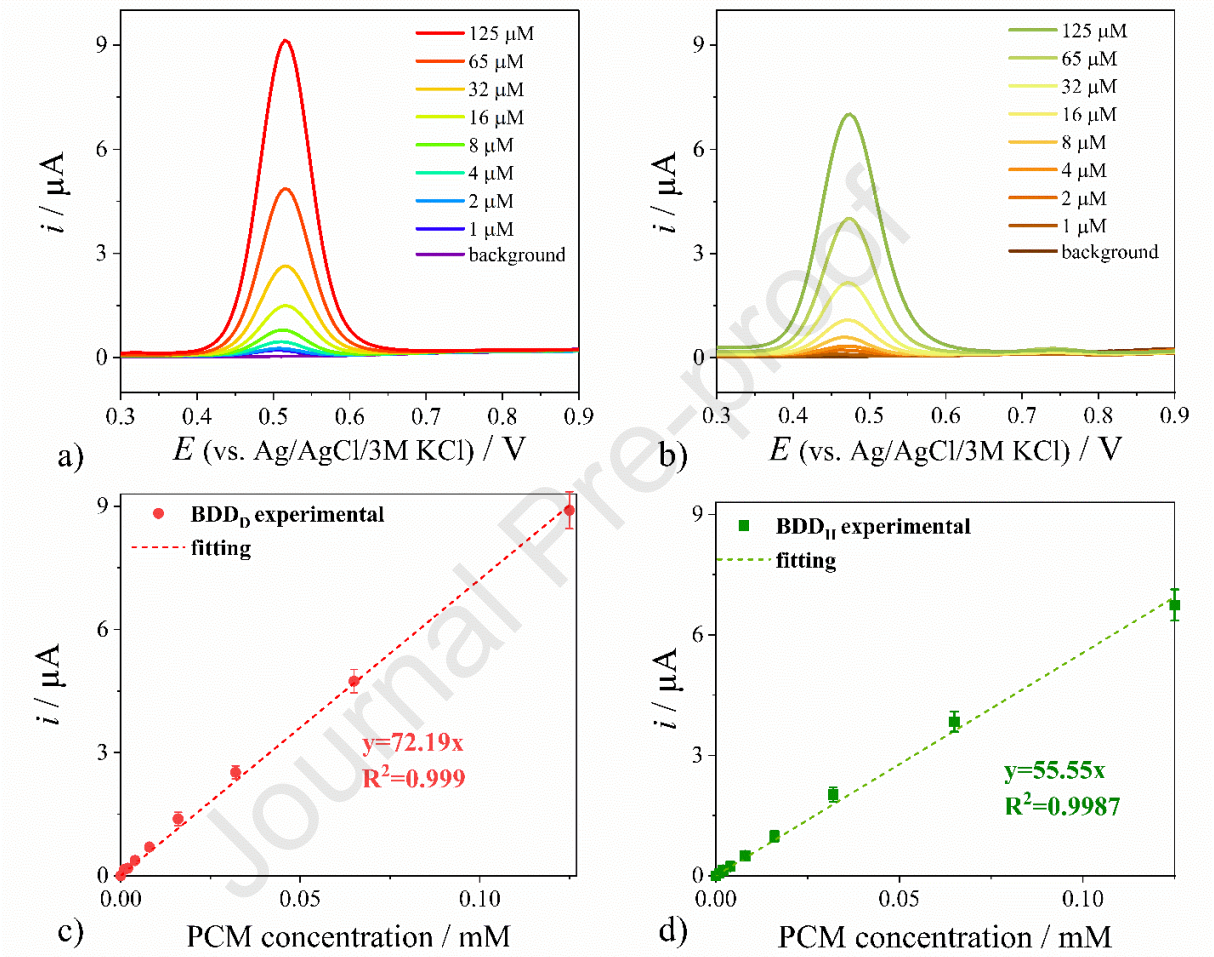

Fig. 7. *DPV of PCM recorded on a) BBD_D, b) BDD_H electrode; and concentration dependence of PCM on c) BDD_D, and d) BDD_H electrode (the error bars represent the standard deviation).*

Table 4. *Comparison of the electroanalytical detection of PCM on different BDD electrodes.*

Electrode	Method	Linear range / µM	LOD / µM	Reference
BDD electrode	*Cyclic Voltammetry*	*100–8000*	*10*	*[82]*
Commercial BDD electrode by Windsor Scientific Ltd.	*DPV*	*10–100*	*0.85*	*[83]*

Cathodically Pretreated Boron-Doped Diamond Electrode	*Square-Wave Voltammetric*	*0.2–97.3*	*-*	*[84]*
BDD electrode	*DPV*	*50–83*	*49*	*[85]*
BDD_H electrode	*DPV*	*1–125*	*2.51*	*This work*
BDD_D electrode	*DPV*	*1–125*	*0.76*	*This work*

4. Conclusions

In summary, the boron-doped diamonds synthesised in the deuterium-rich plasma exhibited activity towards $[Fe(CN)_6]^{3-/4-}$ and $[Ru(NH_3)_6]^{2+/3+}$ redox couples, reaching peak-to-peak separation values of only 60.6 mV, and 59.8 mV, respectively. The substitution of hydrogen to deuterium in the gas phase is primarily responsible for the enhanced boron doping and significantly decrease of nondiamond sp^2 phase in diamond films. This phenomenon is also visible in the Raman spectra followed by a strongly shifted diamond peak from 1332 cm^{-1} to 1312 cm^{-1}, and resistivity of $2.6 \cdot 10^{-3}$ cm. It is worth noting that the amount of (111)-oriented crystals are higher for BDD_D compared to BDD_H. It should also be noted that a low value of background currents leads to an enhanced signal-to-background ratio which allows BDD_D to be used in the application of sensors. The boron-doped diamond grown in deuterium-rich plasma shows very promising electrical and electrochemical properties which can be applied to the thin, sensitive electrochemical sensor with a great linearity range equal to 1–125 µM achieved for PCM.

CRediT authorship contribution statement

A. Dettlaff: Conceptualisation, Methodology, Resources, Investigation, Writing - original draft; **M. Sobaszek:** Conceptualisation, Methodology, Resources, Investigation, Writing - original draft; **T. Klimczuk:** Investigation; **R. Bogdanowicz:** Funding acquisition, Project Administration.

Acknowledgements

The authors express special thanks to Dr. Jacek Ryl and Prof. Tadeusz Ossowski for support. This work was supported by The National Centre for Research and Development Techmatstrateg 347324/12/NCBR/2017. The DS funds of the Faculty of Electronics, Telecommunications and

Informatics of the Gdańsk University of Technology are also acknowledged. *The authors acknowledge Alexander Tools (Gdynia, Poland) for their technical support.*

References

[1] *M.C. Granger, G.M. Swain, The Influence of Surface Interactions on the Reversibility of Ferri/Ferrocyanide at Boron Doped Diamond Thin Film Electrodes, J. Electrochem. Soc. 146 (1999) 4551. https://doi.org/10.1149/1.1392673.*

[2] *M.C. Granger, M. Witek, J. Xu, J. Wang, M. Hupert, A. Hanks, M.D. Koppang, J.E. Butler, G. Lucazeau, M. Mermoux, J.W. Strojek, G.M. Swain, Standard Electrochemical Behavior of High-Quality, Boron-Doped Polycrystalline Diamond Thin-Film Electrodes, Anal. Chem. 72 (2000) 3793–3804. https://doi.org/10.1021/ac0000675.*

[3] *N. Yang, J.S. Foord, X. Jiang, Diamond electrochemistry at the nanoscale: A review, Carbon. 99 (2016) 90–110. https://doi.org/10.1016/j.carbon.2015.11.061.*

[4] *P. Niedziałkowski, Z. Cebula, N. Malinowska, W. Białobrzeska, M. Sobaszek, M. Ficek, R. Bogdanowicz, J.S. Anand, T. Ossowski, Comparison of the paracetamol electrochemical determination using boron-doped diamond electrode and boron-doped carbon nanowalls, Biosens. Bioelectron. 126 (2019) 308–314. https://doi.org/10.1016/j.bios.2018.10.063.*

[5] *S. Garcia-Segura, E. Vieira dos Santos, C.A. Martínez-Huitle, Role of sp3/sp2 ratio on the electrocatalytic properties of boron-doped diamond electrodes: A mini review, Electrochem. Commun. 59 (2015) 52–55. https://doi.org/10.1016/j.elecom.2015.07.002.*

[6] *N.R. Wilson, S.L. Clewes, M.E. Newton, P.R. Unwin, J.V. Macpherson, Impact of Grain-Dependent Boron Uptake on the Electrochemical and Electrical Properties of Polycrystalline Boron Doped Diamond Electrodes, J. Phys. Chem. B. 110 (2006) 5639–5646. https://doi.org/10.1021/jp0547616.*

[7] *A. Deslandes, M.C. Guenette, C.M. Samuell, I. Karatchevtseva, M. Ionescu, D.D. Cohen, B. Blackwell, C. Corr, D.P. Riley, Initial damage processes for diamond film exposure to hydrogen plasma, Fusion Eng. Des. 88 (2013) 3101–3107. https://doi.org/10.1016/j.fusengdes.2013.08.010.*

[8] *A.B. Harker, J.F. DeNatale, Temperature and reactive etching effects on the microstructure of microwave plasma deposited diamond films, J. Mater. Res. 5 (1990) 818–823. https://doi.org/10.1557/JMR.1990.0818.*

[9] *R. Bogdanowicz, M. Sobaszek, M. Sawczak, G.M. Grigorian, M. Ficek, P. Caban, A. Herman, A. Cenian, Enhanced boron doping of thin diamond films grown in deuterium-rich microwave plasma, Diam. Relat. Mater. (2019). https://doi.org/10.1016/j.diamond.2019.05.005.*

[10] *T. Teraji, H. Wada, M. Yamamoto, K. Arima, T. Ito, Highly efficient doping of boron into high-quality homoepitaxial diamond films, Diam. Relat. Mater. 15 (2006) 602–606. https://doi.org/10.1016/j.diamond.2006.01.011.*

[11] *S. Wang, V.M. Swope, J.E. Butler, T. Feygelson, G.M. Swain, The structural and electrochemical properties of boron-doped nanocrystalline diamond thin-film electrodes grown from Ar-rich and H2-rich source gases, Diam. Relat. Mater. 18 (2009) 669–677. https://doi.org/10.1016/j.diamond.2008.11.033.*

[12] R. Issaoui, J. Achard, F. Silva, A. Tallaire, A. Tardieu, A. Gicquel, M.A. Pinault, F. Jomard, Growth of thick heavily boron-doped diamond single crystals: Effect of microwave power density, Appl. Phys. Lett. 97 (2010) 182101. https://doi.org/10.1063/1.3511449.
[13] J.W. Ager, W. Walukiewicz, M. McCluskey, M.A. Plano, M.I. Landstrass, Fano interference of the Raman phonon in heavily boron-doped diamond films grown by chemical vapor deposition, Appl. Phys. Lett. 616 (1995) 616. https://doi.org/10.1063/1.114031.
[14] P. Gonon, E. Gheeraert, A. Deneuville, F. Fontaine, L. Abello, G. Lucazeau, Characterization of heavily B-doped polycrystalline diamond films using Raman spectroscopy and electron spin resonance, J. Appl. Phys. 78 (1995) 7059–7062. https://doi.org/10.1063/1.360410.
[15] V. Mortet, Z.V. Živcová, A. Taylor, M. Davydová, O. Frank, P. Hubík, J. Lorincik, M. Aleshin, Determination of atomic boron concentration in heavily boron-doped diamond by Raman spectroscopy, Diam. Relat. Mater. 93 (2019) 54–58. https://doi.org/10.1016/j.diamond.2019.01.028.
[16] R.J. Zhang, S.T. Lee, Y.W. Lam, Characterization of heavily boron-doped diamond films, Diam. Relat. Mater. 5 (1996) 1288–1294. https://doi.org/10.1016/0925-9635(96)00539-0.
[17] E. Bustarret, E. Gheeraert, K. Watanabe, Optical and electronic properties of heavily boron-doped homo-epitaxial diamond, Phys. Status Solidi A. 199 (2003) 9–18. https://doi.org/10.1002/pssa.200303819.
[18] V. Mortet, I. Gregora, A. Taylor, N. Lambert, P. Ashcheulov, Z. Gedeonova, P. Hubik, New perspectives for heavily boron-doped diamond Raman spectrum analysis, Carbon. (2020) S0008622320306448. https://doi.org/10.1016/j.carbon.2020.06.075.
[19] M. Ficek, M. Sobaszek, M. Gnyba, J. Ryl, Ł. Gołu ski, M. Smietana, J. Jasi ski, P. Caban, R. Bogdanowicz, Optical and electrical properties of boron doped diamond thin conductive films deposited on fused silica glass substrates, Appl. Surf. Sci. 387 (2016) 846–856. https://doi.org/10.1016/j.apsusc.2016.06.165.
[20] D. Ballutaud, F. Jomard, T. Kociniewski, E. Rzepka, H. Girard, S. Saada, Sp3/sp2 character of the carbon and hydrogen configuration in micro- and nanocrystalline diamond, Diam. Relat. Mater. 17 (2008) 451–456. https://doi.org/10.1016/j.diamond.2007.10.004.
[21] K.M. McNamara, K.K. Gleason, D.J. Vestyck, J.E. Butler, Evaluation of diamond films by nuclear magnetic resonance and Raman spectroscopy, Diam. Relat. Mater. 1 (1992) 1145–1155. https://doi.org/10.1016/0925-9635(92)90088-6.
[22] G.M. Swain, Rajeshuni. Ramesham, The electrochemical activity of boron-doped polycrystalline diamond thin film electrodes, Anal. Chem. 65 (1993) 345–351. https://doi.org/10.1021/ac00052a007.
[23] J. Xu, Y. Yokota, R.A. Wong, Y. Kim, Y. Einaga, Unusual Electrochemical Properties of Low-Doped Boron-Doped Diamond Electrodes Containing sp2 Carbon, J. Am. Chem. Soc. 142 (2020) 2310–2316. https://doi.org/10.1021/jacs.9b11183.
[24] T. Watanabe, S. Yoshioka, T. Yamamoto, H. Sepehri-Amin, T. Ohkubo, S. Matsumura, Y. Einaga, The local structure in heavily boron-doped diamond and the effect this has on its electrochemical properties, Carbon. 137 (2018) 333–342. https://doi.org/10.1016/j.carbon.2018.05.026.
[25] J. Ryl, L. Burczyk, R. Bogdanowicz, M. Sobaszek, K. Darowicki, Study on surface termination of boron-doped diamond electrodes under anodic polarization in H2SO4 by

means of dynamic impedance technique, Carbon. 96 (2016) 1093–1105. https://doi.org/10.1016/j.carbon.2015.10.064.

[26] J. Ryl, A. Zielinski, R. Bogdanowicz, K. Darowicki, Heterogeneous distribution of surface electrochemical activity in polycrystalline highly boron-doped diamond electrodes under deep anodic polarization, Electrochem. Commun. 83 (2017) 41–45. https://doi.org/10.1016/j.elecom.2017.08.019.

[27] Yu.V. Pleskov, Yu.E. Evstefeeva, M.D. Krotova, V.P. Varnin, I.G. Teremetskaya, Synthetic semiconductor diamond electrodes: Electrochemical behaviour of homoepitaxial boron-doped films orientated as (111), (110), and (100) faces, J. Electroanal. Chem. 595 (2006) 168–174. https://doi.org/10.1016/j.jelechem.2006.07.010.

[28] P. Hartmann, S. Bohr, R. Haubner, B. Lux, P. Wurzinger, M. Griesser, A. Bergmaier, G. Dollinger, H. Sternschulte, R. Sauer, Diamond growth with boron addition, Int. J. Refract. Met. Hard Mater. 16 (1998) 223–232. https://doi.org/10.1016/S0263-4368(98)00022-5.

[29] X.H. Wang, G.-H.M. Ma, W. Zhu, J.T. Glass, L. Bergman, K.F. Turner, R.J. Nemanich, Effects of boron doping on the surface morphology and structural imperfections of diamond films, Diam. Relat. Mater. 1 (1992) 828–835. https://doi.org/10.1016/0925-9635(92)90109-2.

[30] C.-L. Cheng, H.-C. Chang, J.-C. Lin, K.-J. Song, J.-K. Wang, Direct Observation of Hydrogen Etching Anisotropy on Diamond Single Crystal Surfaces, Phys. Rev. Lett. 78 (1997) 3713–3716. https://doi.org/10.1103/PhysRevLett.78.3713.

[31] W. Gajewski, P. Achatz, O.A. Williams, K. Haenen, E. Bustarret, M. Stutzmann, J.A. Garrido, Electronic and optical properties of boron-doped nanocrystalline diamond films, Phys. Rev. B. 79 (2009) 045206. https://doi.org/10.1103/PhysRevB.79.045206.

[32] K. Ushizawa, K. Watanabe, T. Ando, I. Sakaguchi, M. Nishitani-Gamo, Y. Sato, H. Kanda, Boron concentration dependence of Raman spectra on {100} and {111} facets of B-doped CVD diamond, Diam. Relat. Mater. 7 (1998) 1719–1722. https://doi.org/10.1016/S0925-9635(98)00296-9.

[33] J. V. Macpherson, A practical guide to using boron doped diamond in electrochemical research, Phys. Chem. Chem. Phys. 17 (2015) 2935–2949. https://doi.org/10.1039/C4CP04022H.

[34] N. Habka, E. Chikoidze, F. Jomard, Y. Dumont, J. Chevallier, J. Barjon, C. Mer, P. Bergonzo, Deuterium-induced passivation of boron acceptors in polycrystalline diamond, J. Appl. Phys. 108 (2010) 1–6. https://doi.org/10.1063/1.3518608.

[35] M. Sobaszek, K. Siuzdak, J. Ryl, M. Sawczak, S. Gupta, S.B. Carrizosa, M. Ficek, B. Dec, K. Darowicki, R. Bogdanowicz, Diamond Phase (sp3-C) Rich Boron-Doped Carbon Nanowalls (sp2-C): Physicochemical and Electrochemical Properties, J. Phys. Chem. C. 121 (2017) 20821–20833. https://doi.org/10.1021/acs.jpcc.7b06365.

[36] W. Wang, W. Jacob, J. Roth, Oxidation and hydrogen isotope exchange in amorphous, deuterated carbon films, J. Nucl. Mater. 245 (1997) 66–71. https://doi.org/10.1016/S0022-3115(96)00745-3.

[37] D.G. Onn, A. Witek, Y.Z. Qiu, T.R. Anthony, W.F. Banholzer, Some aspects of the thermal conductivity of isotopically enriched diamond single crystals, Phys. Rev. Lett. 68 (1992) 2806–2809. https://doi.org/10.1103/PhysRevLett.68.2806.

[38] N. Mizuochi, J. Isoya, J. Niitsuma, T. Sekiguchi, H. Watanabe, H. Kato, T. Makino, H. Okushi, S. Yamasaki, Isotope effects between hydrogen and deuterium microwave plasmas

on chemical vapor deposition homoepitaxial diamond growth, J. Appl. Phys. 101 (2007) 103501. https://doi.org/10.1063/1.2727380.

[39] K. Bhardwaj, F. Parvis, Y. Wang, G.J. Blanchard, G.M. Swain, Effect of Surface Oxygen on the Wettability and Electrochemical Properties of Boron-Doped Nanocrystalline Diamond Electrodes in Room-Temperature Ionic Liquids, Langmuir. 36 (2020) 5717–5729. https://doi.org/10.1021/acs.langmuir.0c00294.

[40] J. Ryl, R. Bogdanowicz, P. Slepski, M. Sobaszek, K. Darowicki, Dynamic Electrochemical Impedance Spectroscopy (DEIS) as a Tool for Analyzing Surface Oxidation Processes on Boron-Doped Diamond Electrodes, J. Electrochem. Soc. 161 (2014) H359–H364. https://doi.org/10.1149/2.016406jes.

[41] I. Yagi, H. Notsu, T. Kondo, D.A. Tryk, A. Fujishima, Electrochemical selectivity for redox systems at oxygen-terminated diamond electrodes, J. Electroanal. Chem. 473 (1999) 173–178. https://doi.org/10.1016/S0022-0728(99)00027-3.

[42] L.A. Hutton, J.G. Iacobini, E. Bitziou, R.B. Channon, M.E. Newton, J.V. Macpherson, Examination of the Factors Affecting the Electrochemical Performance of Oxygen-Terminated Polycrystalline Boron-Doped Diamond Electrodes, Anal. Chem. 85 (2013) 7230–7240. https://doi.org/10.1021/ac401042t.

[43] E. Brillas, C.A. Martinez-Huitle, Synthetic Diamond Films: Preparation, Electrochemistry, Characterization, and Applications, John Wiley & Sons, 2011.

[44] M.C. Granger, J. Xu, J.W. Strojek, G.M. Swain, Polycrystalline diamond electrodes: basic properties and applications as amperometric detectors in flow injection analysis and liquid chromatography, Anal. Chim. Acta. 397 (1999) 145–161. https://doi.org/10.1016/S0003-2670(99)00400-6.

[45] R. Bogdanowicz, A. Fabia ska, L. Golunski, M. Sobaszek, M. Gnyba, J. Ryl, K. Darowicki, T. Ossowski, S.D. Janssens, K. Haenen, E.M. Siedlecka, Influence of the boron doping level on the electrochemical oxidation of the azo dyes at Si/BDD thin film electrodes, Diam. Relat. Mater. 39 (2013) 82–88. https://doi.org/10.1016/j.diamond.2013.08.004.

[46] T.A. Ivandini, T. Watanabe, T. Matsui, Y. Ootani, S. Iizuka, R. Toyoshima, H. Kodama, H. Kondoh, Y. Tateyama, Y. Einaga, Influence of Surface Orientation on Electrochemical Properties of Boron-Doped Diamond, J. Phys. Chem. C. 123 (2019) 5336–5344. https://doi.org/10.1021/acs.jpcc.8b10406.

[47] C. Batchelor-McAuley, K. Ngamchuea, R.G. Compton, Simulated low-support voltammetry: Deviations from Ohm's Law, J. Electroanal. Chem. 830–831 (2018) 88–94. https://doi.org/10.1016/j.jelechem.2018.10.032.

[48] P. Charoen-amornkitt, T. Suzuki, S. Tsushima, Ohmic resistance and constant phase element effects on cyclic voltammograms using a combined model of mass transport and equivalent circuits, Electrochimica Acta. 258 (2017) 433–441. https://doi.org/10.1016/j.electacta.2017.11.079.

[49] J. Wang, Analytical Electrochemistry, Third, WILEY-VCH, 2006.

[50] P. Actis, A. Denoyelle, R. Boukherroub, S. Szunerits, Influence of the surface termination on the electrochemical properties of boron-doped diamond (BDD) interfaces, Electrochem. Commun. 10 (2008) 402–406. https://doi.org/10.1016/j.elecom.2007.12.032.

[51] A. Zielinski, M. Cieslik, M. Sobaszek, R. Bogdanowicz, K. Darowicki, J. Ryl, Multifrequency nanoscale impedance microscopy (m-NIM): A novel approach towards detection of selective and subtle modifications on the surface of polycrystalline boron-

doped diamond electrodes, Ultramicroscopy. 199 (2019) 34–45. https://doi.org/10.1016/j.ultramic.2019.01.004.

[52] J. Ryl, L. Burczyk, A. Zielinski, M. Ficek, A. Franczak, R. Bogdanowicz, K. Darowicki, Heterogeneous oxidation of highly boron-doped diamond electrodes and its influence on the surface distribution of electrochemical activity, Electrochimica Acta. 297 (2019) 1018–1027. https://doi.org/10.1016/j.electacta.2018.12.050.

[53] A.J. Bard, L.R. Faulkner, Electrochemical Methods: Fundamentals and Applications, 2 edition, Wiley, New York, 2000.

[54] O. Hammerich, B. Speiser, eds., Organic Electrochemistry: Revised and Expanded, 5 edition, CRC Press, Boca Raton, 2015.

[55] H. Matsuda, Y. Ayabe, Zur Theorie der Randles-Sev ikschen Kathodenstrahl-Polarographie, Z. Für Elektrochem. Berichte Bunsenges. Für Phys. Chem. 59 (1955) 494–503. https://doi.org/10.1002/bbpc.19550590605.

[56] R.G. Compton, C.E. Banks, Understanding Voltammetry (Third Edition), World Scientific, 2018.

[57] R.S. Nicholson, Theory and Application of Cyclic Voltammetry for Measurement of Electrode Reaction Kinetics., Anal. Chem. 37 (1965) 1351–1355. https://doi.org/10.1021/ac60230a016.

[58] A.J. Bard, L.R. Faulkner, Electrochemical Methods. Fundamentals and Appliactions., Second, John Wiley @ Sons, INC., 2001. https://doi.org/10.1016/j.aca.2010.06.020.

[59] Y. Wang, J.G. Limon-Petersen, R.G. Compton, Measurement of the diffusion coefficients of [Ru(NH3) 6]3+ and [Ru(NH3)6]2+ in aqueous solution using microelectrode double potential step chronoamperometry, J. Electroanal. Chem. 652 (2011) 13–17. https://doi.org/10.1016/j.jelechem.2010.12.011.

[60] T.J. Davies, C.E. Banks, R.G. Compton, Voltammetry at spatially heterogeneous electrodes, J. Solid State Electrochem. 9 (2005) 797–808. https://doi.org/10.1007/s10008-005-0699-x.

[61] C. Amatore, J.M. Saveant, D. Tessier, Charge transfer at partially bloced surfaces, J Electroanal Chem. 147 (1983) 39–51.

[62] T.J. Davies, E.R. Lowe, S.J. Wilkins, R.G. Compton, Voltammetric sizing of inert particles, ChemPhysChem. 6 (2005) 1340–1347. https://doi.org/10.1002/cphc.200500152.

[63] J. Ryl, L. Burczyk, A. Zielinski, M. Ficek, A. Franczak, R. Bogdanowicz, K. Darowicki, Heterogeneous oxidation of highly boron-doped diamond electrodes and its in fl uence on the surface distribution of electrochemical activity, Electrochimica Acta. 297 (2019) 1018–1027. https://doi.org/10.1016/j.electacta.2018.12.050.

[64] B. Hirschorn, M.E. Orazem, B. Tribollet, V. Vivier, I. Frateur, M. Musiani, Determination of effective capacitance and film thickness from constant-phase-element parameters, Electrochimica Acta. 55 (2010) 6218–6227. https://doi.org/10.1016/j.electacta.2009.10.065.

[65] J. Wysocka, M. Cieslik, S. Krakowiak, J. Ryl, Carboxylic acids as efficient corrosion inhibitors of aluminium alloys in alkaline media, Electrochimica Acta. 289 (2018) 175–192. https://doi.org/10.1016/j.electacta.2018.08.070.

[66] J. Wysocka, S. Krakowiak, J. Ryl, Evaluation of citric acid corrosion inhibition efficiency and passivation kinetics for aluminium alloys in alkaline media by means of dynamic impedance monitoring, Electrochimica Acta. 258 (2017) 1463–1475. https://doi.org/10.1016/j.electacta.2017.12.017.

[67] *Y.V. Pleskov, Synthetic diamond in electrochemistry, Russ. Chem. Rev. 68 (1999) 381–392. https://doi.org/10.1070/RC1999v068n05ABEH000494.*
[68] *E. Luais, M. Boujtita, A. Gohier, A. Tailleur, S. Casimirius, M.A. Djouadi, A. Granier, P.Y. Tessier, Carbon nanowalls as material for electrochemical transducers, Appl. Phys. Lett. 95 (2009) 1–4. https://doi.org/10.1063/1.3170033.*
[69] *K. Siuzdak, M. Ficek, M. Sobaszek, J. Ryl, M. Gnyba, P. Niedziałkowski, N. Malinowska, J. Karczewski, R. Bogdanowicz, Boron-Enhanced Growth of Micron-Scale Carbon-Based Nanowalls: A Route toward High Rates of Electrochemical Biosensing, ACS Appl. Mater. Interfaces. 9 (2017) 12982–12992. https://doi.org/10.1021/acsami.6b16860.*
[70] *Shokoofeh. Alehashem, Fred. Chambers, J.W. Strojek, G.M. Swain, Rajeshuni. Ramesham, Cyclic Voltammetric Studies of Charge Transfer Reactions at Highly Boron-Doped Polycrystalline Diamond Thin-Film Electrodes, Anal. Chem. 67 (1995) 2812–2821. https://doi.org/10.1021/ac00113a014.*
[71] *M.C. Granger, J. Xu, J.W. Strojek, G.M. Swain, Polycrystalline diamond electrodes: basic properties and applications as amperometric detectors in flow injection analysis and liquid chromatography, Anal. Chim. Acta. 397 (1999) 145–161.*
[72] *G.M. Swain, R. Ramesham, The electrochemical activity of boron-doped polycrystalline diamond thin film electrodes, Anal. Chem. 65 (1993) 345–351. https://doi.org/10.1021/ac00052a007.*
[73] *R. Bogdanowicz, Influence of the boron doping level on the electrochemical oxidation of the azo dyes at Si/BDD thin film electrodes, Diam. Relat. Mater. (2013) 82–88.*
[74] *R. Šelešovská, B. Kränková, M. Št pánková, P. Martinková, L. Janíková, J. Chýlková, M. Vojs, Influence of boron content on electrochemical properties of boron-doped diamond electrodes and their utilization for leucovorin determination, J. Electroanal. Chem. 821 (2018) 2–9. https://doi.org/10.1016/j.jelechem.2018.02.007.*
[75] *L.A. Hutton, J.G. Iacobini, E. Bitziou, R.B. Channon, M.E. Newton, J.V. Macpherson, Examination of the Factors Affecting the Electrochemical Performance of Oxygen-Terminated Polycrystalline Boron-Doped Diamond Electrodes, Anal. Chem. 85 (2013) 7230–7240. https://doi.org/10.1021/ac401042t.*
[76] *R.F. Teófilo, H.J. Ceragioli, A.C. Peterlevitz, L.M. Da Silva, F.S. Damos, M.M.C. Ferreira, V. Baranauskas, L.T. Kubota, Improvement of the electrochemical properties of "as-grown" boron-doped polycrystalline diamond electrodes deposited on tungsten wires using ethanol, J. Solid State Electrochem. 11 (2007) 1449–1457. https://doi.org/10.1007/s10008-007-0319-z.*
[77] *B.C. Lourencao, T.A. Silva, H. Zanin, P.W. May, E.J. Corat, O. Fatibello-Filho, Promising electrochemical performance of high-surface-area boron-doped diamond/carbon nanotube electroanalytical sensors, J. Solid State Electrochem. 20 (2016) 2403–2409. https://doi.org/10.1007/s10008-016-3128-4.*
[78] *A. Dettlaff, P. Jakóbczyk, M. Ficek, B. Wilk, M. Szala, J. Wojtas, T. Ossowski, R. Bogdanowicz, Electrochemical determination of nitroaromatic explosives at boron-doped diamond/graphene nanowall electrodes: 2,4,6-trinitrotoluene and 2,4,6-trinitroanisole in liquid effluents, J. Hazard. Mater. 387 (2020) 121672. https://doi.org/10.1016/j.jhazmat.2019.121672.*
[79] *. Sa lam, A. Üzer, E. Erça , R. Apak, Electrochemical Determination of TNT, DNT, RDX, and HMX with Gold Nanoparticles/Poly(Carbazole-Aniline) Film–Modified Glassy Carbon Sensor Electrodes Imprinted for Molecular Recognition of Nitroaromatics and*

Nitramines, Anal. Chem. 90 (2018) 7364–7370. https://doi.org/10.1021/acs.analchem.8b00715.

[80] A. Shrivastava, V. Gupta, Methods for the determination of limit of detection and limit of quantitation of the analytical methods, Chron. Young Sci. 2 (2011) 21–21.

[81] Yu.V. Pleskov, Yu.E. Evstefeeva, M.D. Krotova, V.P. Varnin, I.G. Teremetskaya, Synthetic semiconductor diamond electrodes: Electrochemical behaviour of homoepitaxial boron-doped films orientated as (111), (110), and (100) faces, J. Electroanal. Chem. 595 (2006) 168–174. https://doi.org/10.1016/j.jelechem.2006.07.010.

[82] N. Wangfuengkanagul, O. Chailapakul, Electrochemical analysis of acetaminophen using a boron-doped diamond thin film electrode applied to flow injection system, J. Pharm. Biomed. Anal. 28 (2002) 841–847. https://doi.org/10.1016/S0731-7085(01)00695-1.

[83] C. Radovan, C. Cofan, D. Cinghita, Simultaneous Determination of Acetaminophen and Ascorbic Acid at an Unmodified Boron-Doped Diamond Electrode by Differential Pulse Voltammetry in Buffered Media, Electroanalysis. 20 (2008) 1346–1353. https://doi.org/10.1002/elan.200804188.

[84] A.M. Santos, F.C. Vicentini, P.B. Deroco, R.C. Rocha-Filho, O. Fatibello-Filho, Square-Wave Voltammetric Determination of Paracetamol and Codeine in Pharmaceutical and Human Body Fluid Samples Using a Cathodically Pretreated Boron-Doped Diamond Electrode, J. Braz. Chem. Soc. (2015). https://doi.org/10.5935/0103-5053.20150203.

[85] B.C. Lourenção, R.A. Medeiros, R.C. Rocha-Filho, L.H. Mazo, O. Fatibello-Filho, Simultaneous voltammetric determination of paracetamol and caffeine in pharmaceutical formulations using a boron-doped diamond electrode, Talanta. 78 (2009) 748–752. https://doi.org/10.1016/j.talanta.2008.12.040.

Highlights:

- Novel deuterium-plasma-grown diamond electrodes were prepared.
- Deuterium enriched electrode exhibited high electroactivity and stability.
- Enhanced electrochemical mechanism of the diamond electrodes was elaborated.
- Wide linear range of sensing of paracetamol from 1 to 125 µM was achieved.